H1prelim-21-032
July 2021
Submitted to ISMD2021 and EPS-HEP21 conferences

Measurement of the 1-jettiness event shape observable in deep-inelastic electron-proton scattering at HERA

H1 Collaboration

Abstract

A first measurement of the 1-jettiness event shape observable in neutral-current deep-inelastic electron-proton scattering is presented. The 1-jettiness observable τ_b^1 is defined such that it is equivalent to the thrust observable defined in the Breit frame. The data were taken in the years 2003 to 2007 with the H1 detector at the HERA ep collider at a center-of-mass energy of 319 GeV and correspond to an integrated luminosity of $351.6\,\mathrm{pb}^{-1}$. The triple-differential cross sections are presented as a function of the 1-jettiness τ_b^1, the event virtuality Q^2 and the inelasticity y in the kinematic region $Q^2 > 150\,\mathrm{GeV}^2$. The data have sensitivity to the parton distribution functions of the proton, the strong coupling constant and to resummation and hadronisation effects. The data are compared to selected predictions.

1 Digest

A variety of event shape observables have been measured in neutral-current deep-inelastic scattering (NC DIS) in the past in electron-proton collisions by the H1 experiment [1–3] and by ZEUS [4, 5]. They have proven to exhibit an interesting sensitivity to the strong coupling constant, $\alpha_s(m_Z)$, to hadronisation and to resummation effects. Due to their close relation to inclusive DIS cross sections they also have sensitivity to the parton distribution functions of the proton (PDFs) [6]. An event shape observable of particular interest is the thrust $\tau = 1 - T$, which measures the sum of the longitudinal momentum components of the hadronic final state particles in the current hemisphere. In this quantity, the current hemisphere $\mathcal{H}_\mathcal{C}$ defines the region in the Breit frame [7] with $\eta < 0$. The *hadronic final state* (HFS) refers to all final-state particles in the event that are not the scattered lepton.

There are different definitions of the thrust, differing in the normalisation parameter. The definition in which the total longitudinal momentum in the current hemisphere of the Breit frame is normalised to $Q/2$ is of particular interest for precise and stable theoretical predictions [8–10]:

$$\tau_Q = 1 - \frac{2}{Q} \sum_{i \in \mathcal{H}_\mathcal{C}} P_{z,i}^{\text{Breit}} \,. \tag{1}$$

The denominator Q denotes the square-root of the virtuality $Q = \sqrt{-q^2}$, where q is the four-vector of the exchanged boson, $P_{z,i}^{\text{Breit}}$ are the longitudinal momenta of the HFS particles in the current hemisphere $\mathcal{H}_\mathcal{C}$. This definition is infrared safe, allows for analytic or automatised resummation and is free of non-global logarithms [11]. With the rise of soft-collinear effective theory (SCET), it was recognised that τ_Q has an equivalence with a global event-shape observable in terms of a 1-jettiness observable [12, 13]

$$\tau_1^b = \frac{2}{Q^2} \sum_{i \in X} \min\{xP \cdot p_i, (q + xP) \cdot p_i\} \,. \tag{2}$$

The quantity x denotes the Bjorken-scaling variable, P is the proton beam four-vector and p_i are the four-vectors of the HFS particles. Differently than for τ_Q, the summation index in the definition of τ_1^b runs over the HFS particles in both current and beam hemispheres. The τ_1^b is a Lorentz invariant observable, thus the quantity can be evaluated directly in the laboratory frame. From energy-momentum conservation it is found that [13]

$$\tau_Q = \tau_1^b \,. \tag{3}$$

Since both definitions are equivalent, the 1-jettiness τ_1^b can be measured as τ_Q. Therefore, only the particles in the current hemisphere are considered, while the particles in the beam hemisphere do not contribute directly to the observable τ_Q.

The data was taken in the years 2003 to 2007 using electron or positron beams at a center-of-mass energy of $\sqrt{s} = 319\,\text{GeV}$, and correspond to an integrated luminosity of $\mathcal{L} = 351.6\,\text{pb}^{-1}$ [14]. The events are triggered by a high-energetic cluster in the liquid argon calorimeter (LAr). The efficiency is larger than 99 % for an inclusive DIS sample in the given phase space [15], if the scattered electron energy exceeds $E_{e'} > 11\,\text{GeV}$.

A number of requirements to suppress non-collision background from beam-gas interaction or beam-halo are applied [15, 16], as well as to suppress QED compton events [15]. A particle-flow

algorithm is employed for the reconstruction of individual particle candidates, which combines the information from tracks with clusters. Their energy is calibrated using a neural-network based shower-classification algorithm and a dedicated jet-calibration sample [17].

At detector-level in data and particle-level[1], the data are required to have a longitudinal energy-momentum balance between $45 < (E - P_z)_{\text{tot}} < 65\,\text{GeV}$, which is defined from a sum over all particles as $(E - P_z)_{\text{tot}} = \sum_{e',i\in X}(E_i - P_{z,i})$. This requirement reduces effects from initial state QED radiation (ISR).

The DIS kinematic variables are defined from the IΣ-method [18, 19]:

$$Q^2 = Q^2_\Sigma = \frac{E^2_{e'}\sin^2\theta_{e'}}{1 - y_\Sigma}\,, \quad y = y_\Sigma = \frac{\Sigma}{\Sigma + E_{e'}(1 - \cos\theta_{e'})} \quad \text{and} \quad x = x_{\text{I}\Sigma} = \frac{E_{e'}}{E_p}\frac{\cos^2(\theta_{e'}/2)}{y_\Sigma}\,. \tag{4}$$

The quantity Σ is defined as $\Sigma = \sum_{i\in X}(E_i - P_{z,i})$, the polar angle of the scattered electron is denoted $\theta_{e'}$, and E_p is the proton beam energy $E_p = 920\,\text{GeV}$. The Bjorken variable x is required to define the boost-vector to the Breit frame. The IΣ method has the advantage that the electron-beam energy does not enter into the equations. Thus they are largely insensitive to initial state QED radiative effects. In addition, it was found that the IΣ method yields highest purities for most of the bins in the measured phase space, as compared to other reconstruction methods.

The polar-angle acceptance of the LAr, $\theta \lesssim 154°$, defines the Q^2-region of the measurement and thus $Q^2 > 150\,\text{GeV}^2$. The electron-energy requirement translates roughly to $y \lesssim 0.7$. The region $y \lesssim 0.1$ (which corresponds to high-x) is omitted from the measurement, as this kinematic regime cannot be well measured due to limited acceptance and resolution in the very forward region. In addition, the Lorentz-factor β of the boost vector approaches unity.

The data are corrected for detector effects, background processes and higher-order QED effects at the lepton-vertex, as described in the following. Cross sections $d\sigma/d\tau_1^b(Q^2, y) = \int_{\Delta Q^2\Delta y} \frac{d\sigma}{dQ^2 dy d\tau}$ are measured in each (Q^2, y) bin as

$$\sigma = \frac{N_{\text{data}} - N_{\text{Bkg}}}{\mathcal{L}\cdot\Delta_\tau}\cdot c_{\text{unfold}}\cdot c_{\text{QED}}\,, \tag{5}$$

where N_{data} denotes the number of data events, N_{Bkg} denotes the estimated number of events from processes other than high-Q^2 inclusive NC DIS, Δ_τ denotes the bin-width in τ_1^b, c_{unfold} is the detector-correction factor, c_{QED} denotes the QED corrections. The data are corrected for acceptance and resolution effects of the detector using the bin-by-bin method (denoted as *unfolding*) and the correction factors c_{unfold} are obtained from two *signal* Monte Carlo models Djangoh [20] and Rapgap [21] (see below) together with a detailed simulation of the H1 detector based on GEANT3 [22]. Altogether more than 4×10^8 events are simulated for that purpose. All technical aspects of the detector are well modelled, and both MC models provide an accurate description of the data; the two models based on different physics models commonly bracket the data. A comparison of the data and these simulations for selected observables is displayed in figs. 1 and 2. The data are further corrected for QED radiative effects, where multiplicative factors c_{QED} are derived using Djangoh and Rapgap. Both models implement higher-order

[1]The particle-level used for the unfolding includes higher-order QED radiation at the lepton-vertex. In these *radiative* MC events, ISR photons are not included into the calculation of $(E-P_z)_{\text{tot}}$ at particle-level. In contrast, in non-radiative MC this cut is not applicable and one always finds $(E - P_z)_{\text{tot}} = 2E_e$.

QED effects with the subroutines from Heracles [23]. The QED effects corrected for include the emission of photons from the lepton line, photonic lepton vertex corrections, self-energy contributions at the external lepton lines, but not for fermionic contributions to the running of the electromagnetic coupling. The number of events from processes other than high-Q^2 inclusive DIS, N_{Bkg}, are obtained from simulated events of low-Q^2 NC DIS (Djangoh, $4 < Q^2 < 60\,\mathrm{GeV}^2$), photoproduction (Pythia 6.2 [24, 25], $Q^2 < 4\,\mathrm{GeV}^2$), charged current DIS (Djangoh), QED Compton events (Compton [26]), while the contributions from di-lepton production (Grape [27]), charged current DIS (Djangoh) and deeply virtual Compton scattering (TinTin/Milou) are found to be negligible. The name in the parenthesis denotes the respective MC event generator program used.

To the measurement of τ_Q all particle candidates in the current hemisphere in every selected NC DIS event contribute, see eq. (1). Therefore a detailed understanding of the acceptance and resolution of all single particles is of importance, and a precise modelling of the detector response is required for an unbiased unfolding. The distribution of the longitudinal momentum in the Breit frame of all particle-candidates P_z^{Breit} in the selected events are compared with the simulations in fig. 3, separately for reconstructed clusters (left) or tracks (right). Overall, good agreement between the simulation and the data is observed, both, for clusters and tracks. The contribution from individual particle-candidates to τ_Q in different θ-regions or different particle energies E are displayed in figs. 4 and 5. It is observed that the most relevant contributions are from objects in the central part of the detector ($25 < \theta < 153^\circ$) and from objects with large energy ($E > 1.0\,\mathrm{GeV}$). Both can be well measured with the various subdetector components of the H1 detector [28–31]. The simulations provide an accurate description of the data altogether.

The measurement is associated with a number of systematic uncertainties from various sources. These are briefly summarised in the following:

- The energies of all clusters and tracks receive final calibration factors from a dedicated jet-energy calibration [15, 17]. This calibration procedure results in two independent uncertainty contributions, denoted as 'jet energy scale uncertainty' (JES) and 'remaining cluster energy scale uncertainty' (RCES). Both uncertainties are determined by varying the energy of the HFS objects by 1 %. The JES rather affects high-energetic objects, while the RCES rather affects low-P_{T} objects.
- The energy of the scattered lepton is measured with a precision of 0.5 % in the central and backward region of the detector, and with 1 % precision in the forward region of the detector [32].
- The polar-angle position of the LAr with respect to the Central Tracking Detector (CTD) is aligned with a precision of 1 mrad [32]. This uncertainty component is considered separately for the scattered electron and for the HFS objects.
- The integrated luminosity is associated with an uncertainty of 2.7 % [14].

Various predictions are compared to the measured cross sections

- The DIS MC event generator Djangoh 1.4 [20] which implements higher-order QCD radiation through the color-dipole model as implemented in Ariadne [33]. The Lund string fragmentation model [34, 35] with the ALEPH tune [36] and the CTEQ6L PDF [37] are used. Higher-order QED radiation is simulated with the Heracles program [23], although this is used only for radiative MC events used for unfolding, but not for the cross section predictions.

- The DIS MC event generator Rapgap 3.1 [21], which implements parton showers in the leading-logarithmic approximation. Similarly as Djangoh, Heracles, the Lund string fragmentation model with the ALEPH tune, and the CTEQ6L is implemented.
- The MC event generator Pythia 8.303 [38, 39] is used together with the NNPDF3.1 PDF set [40]. The value of the strong coupling constant is set consistently to 0.118. Three different parton-shower models are studied: i) the 'default' dipole-like $p_\perp$-ordered shower, ii) the $p_\perp$-ordered Vincia parton shower [41–44] at leading color, and ii) the Dire [45–47] parton shower which is an improved dipole-shower with additional handling of collinear enhancements. The Pythia 8.3 default for hadronisation is used [39].
- The MC event generator Herwig 7.2 [48] is used with its default settings, and the events are analysed with Rivet [49].
- Next-to-next-to-leading order predictions in perturbative QCD for the process $ep \to e + 2\text{jets} + X$ are obtained with the program NNLOJET [50–53]. The factorisation and renormalisation scales are identified with $\mu = Q$. Scale uncertainties are obtained as the largest difference in the 7-point scale-variation prescription with scale factors 0.5 and 2. The PDF set NNPDF3.1 [40] is used. Non-perturbative correction factors are applied to these parton-level predictions and multiplicative correction factors for hadronisation effects are obtained from Pythia 8.3. These NNLO predictions are valid only in the region where the $2 \to 2$ process dominates and hadronisation corrections are small, and thus aproximately $\tau_1^b \gtrsim 0.22$ and $\tau_1^b \neq 1$. From the same program, also NLO predictions are obtained and are displayed for comparison.

2 Results

The 1-jettiness cross sections are measured as single-differential cross sections $d\sigma/d\tau_1^b$ in two variants. In both cases, the full τ_1^b spectra is measured and no further cuts are applied, so τ_1^b is measured in the range $0 \leq \tau_1^b \leq 1$. Consequently, if all bins in τ_1^b are integrated, one obtains the bin-integrated inclusive NC DIS cross section in the respective Q^2 and y interval. First, single-differential cross sections $d\sigma/d\tau_1^b$ are measured in 13 bins in τ_1^b in a large kinematic region

$$150 < Q^2 < 20\,000\,\text{GeV}^2 \quad \text{and} \quad 0.2 < y < 0.7\,. \tag{6}$$

These are referred to as *single-differential cross sections* in the following. Secondly, $d\sigma/d\tau_1^b$ is measured for adjacent smaller intervals in Q^2 and y in the range

$$150 < Q^2 < 20\,000\,\text{GeV}^2 \quad \text{and} \quad 0.1 < y < 0.9\,, \tag{7}$$

where (Q^2,y)-intervals with low purities or data points with large statistical uncertainties are omitted. These cross sections are referred to as *triple-differential cross sections* in the following.

The single-differential cross sections $d\sigma/d\tau_1^b$ are presented in figs. 6 and 7 and compared to various predictions, as described in the caption of the figures. The τ_1^b cross section exhibits a distinct peak at around $\tau_1^b \sim 0.15$ and a tail towards high values of τ_1^b. The peak region is related to DIS born-level kinematics and subject to hadronisation and resummation effects, while the tail region is populated by events with additional hard radiation. The highest bin at $\tau_1^b \sim 1$ has a sizeable cross section, and these are from events that have no particles in the current hemisphere in the Breit frame.

The classical MC event generators Djangoh and Rapgap provide an overall reasonable description of the data, although the region of low τ_1^b is underestimated by both models. The high τ_1^b region is well described, and Djangoh is a bit higher than Rapgap, which is related to its harder P_T-spectra of jets [54]. The MC predictions from Pythia+Dire provide a somewhat reasonable description. In particular, the peak region at $\tau_1^b \sim 0.15$ is better described than by Djangoh or Rapgap, but the tail-region at high τ_1^b is underestimated by Pythia+Dire. Vinca and the Pythia-default parton shower provide a similar description of the high-τ_1^b region than Dire, but Vincia overestimates the peak-region, whereas the default-shower is better in normalisation but fails to describe the shape of the peak-region. The NNLO predictions provide an improved description of the data as compared to Pythia+Dire, although the bulk region remains somewhat underestimated. The NNLO predictions provide an improved description of the data as compared to NLO predictions, and the NLO predictions are altoghether quite similar to Pythia+Dire.

The triple-differential cross sections are presented in figs. 8, 10 and 12, and the ratio to the data are displayed in figs. 9, 11 and 13. With increasing Q^2, the peak of the distribution shifts towards lower values of τ_1^b, which is related to the increasing momentum of the DIS born-level jet, and a reduced importance of hadronisation effects. Similarly, at higher Q^2, the high τ_1^b region is of less importance. Furthermore, the cross section at $\tau_1^b \sim 1$ reduces with increasing Q^2. This region is dominated by event topologies without particles in the current hemisphere, which is related to events with x at least smaller than 0.5 [13]. This configuration is present because DIS is a hadron-initiated process and τ_1^b is defined in the Breit frame, whereas such configurations do not exist in the equivalent definition of τ_1^b in e^+e^- collisions [55].

The triple-differential cross sections are best described by Djangoh. Rapgap underestimates the high τ_1^b region at low y. Pythia+Dire is similar to Rapgap at low-y but has additionally a too high peak at low τ_1^b, and underestimates the data at high τ_1^b. The other parton-shower models interfaced to Pythia are similar to Dire, and the main difference is at low τ_1^b, where all models overestimate the data at lower Q^2. The Herwig predictions are often similar to those from Pythia, but they have two features: in the low τ_1^b region the data are underestimated, and there is a prominent structure in the τ_1^b spectrum at medium τ_1^b that changes with y. The NNLO predictions provide a good description of the data at $\tau_1^b \sim 0.35$ and underestimate the data at higher τ_1^b. The sizable NP corrections limit may be a limiting factor and need to be investigated in detail. The NNLO predictions provide an improved description as compared to Pythia+Dire or NLO predictions. The latter are altogether similar to Pythia+Dire in the region of validity.

3 Summary and conclusion

A first measurement of the 1-jettiness event shape observable in neutral-current deep-inelastic electron-proton scattering at HERA is presented using data taken with the H1 experiment. The 1-jettiness observable τ_1^b is equivalent to the classical event shape observable τ_Q. The cross sections are measured as a function of τ_1^b in the kinematic region $150 < Q^2 < 20\,000\,\mathrm{GeV}^2$ and $0.2 < y < 0.7$, and in a triple-differential manner in the region $150 < Q^2 < 20\,000\,\mathrm{GeV}^2$ and $0.1 < y < 0.9$. The data are compared to various predictions, while only the classical Monte Carlo event generators Djangoh and Rapgap provide a satisfactory description. The data will be valuable for optimisation of multi-purpose MC event generators, and the data is sensitive to the value of the strong coupling constant, to hadronisation and resummation effects and to parton-distribution functions of the proton.

4 Figures

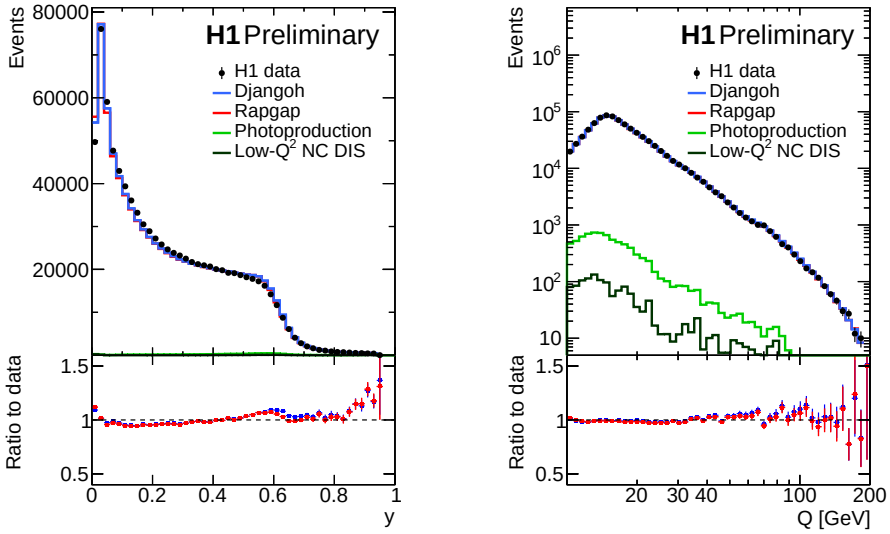

Figure 1: Detector level distributions of y (left) and Q (right) of all pre-selected data. The definition of these observables is given in the Equations (4).The data are compared to simulated data using the MC generators Djangoh and Rapgap. Further simulated data with different processes are added to both models. The most relevant background processes are low-Q^2 NC DIS ($Q^2 < 60\,\mathrm{GeV}^2$) and photoproduction, displayed in a stacked style. Other processes are found to be negligble and hence the photoproduction represents the sum of all *background* processes.

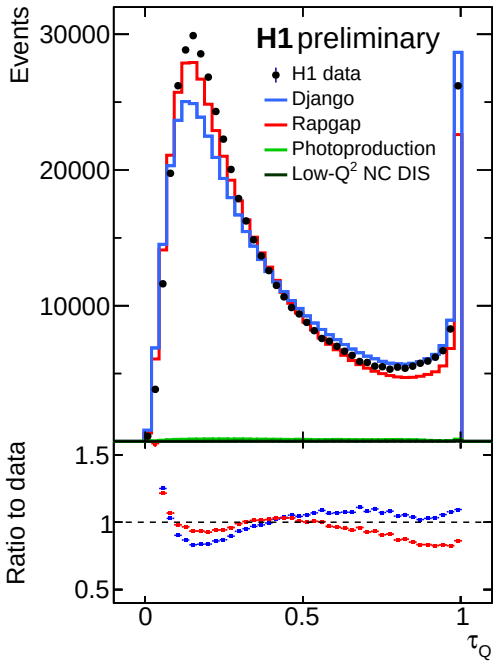

Figure 2: Detector-level distribution of τ_Q, of the pre-selected data and in the range $150 < Q^2 < 20\,000\,\mathrm{GeV}^2$ and $0.2 < y < 0.7$. The data are compared to simulated data using Djangoh or Rapgap, and to both models various other background processes are added (green line, see fig. 1 for further details). The signal MC models provide a satisfactory description of the data and bracket the data. The simulation of the experimental apparatus is found to be very satisfactory.

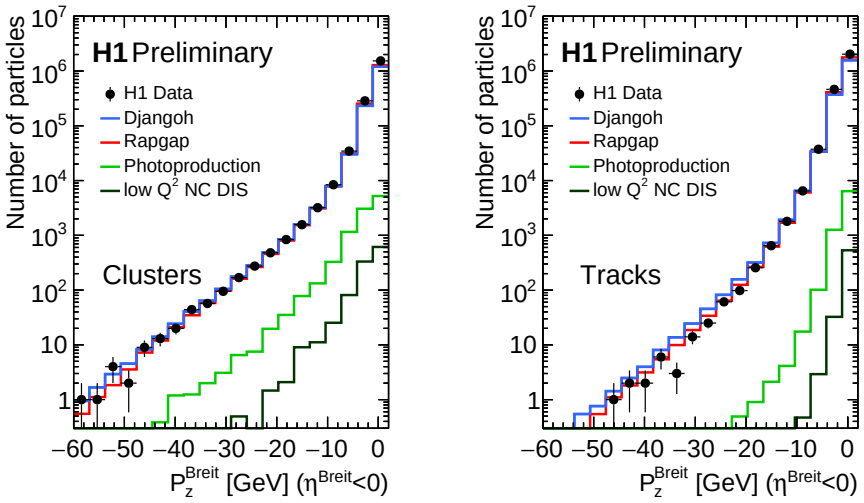

Figure 3: The longitudinal momentum P_z^{Breit} in the Breit frame of reconstructed particle candidates (denoted as *particles*) in the selected events. Only particle candidates with $\eta^{\mathrm{Breit}} < 0$ are displayed, since only those contribute to the actual calculation of τ_Q. Particle candidates are defined by an energy-flow algorithm taking clusters and tracks into account. Left: the P_z^{Breit} distribution for clusters, right: the P_z^{Breit} distribution for tracks. The detector-level data are compared to signal MC models Djangoh and Rapgap, which include further MC samples for background processes (see text).

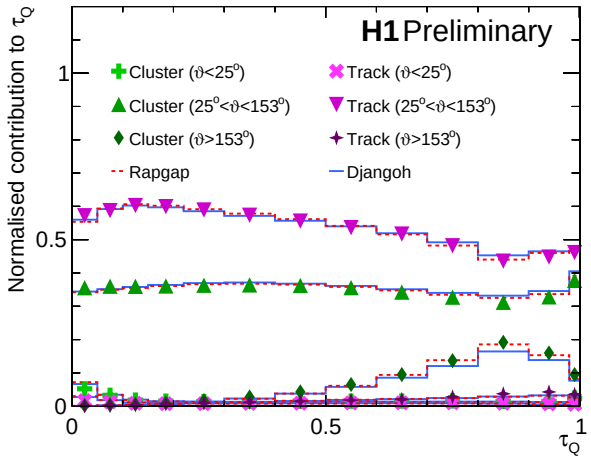

Figure 4: The normalised contribution to τ_Q for differently reconstructed particle candidates (tracks or clusters) in three distinct polar regions θ. The regions are chosen according to θ-ranges, where different components of the H1 detector are relevant for particle reconstruction [28–31]. The data are compared to the signal MC models Djangoh and Rapgap. Good agreement between the simulation and the data are observed. The relative contributions are obtained by calculating a weight $w = \sum_{\text{contrib}} P_z^{\text{Breit}} / \sum_{\text{all}} P_z^{\text{Breit}}$ for every event and every contribution. The resulting distributions are normalised with the τ_Q distribution.

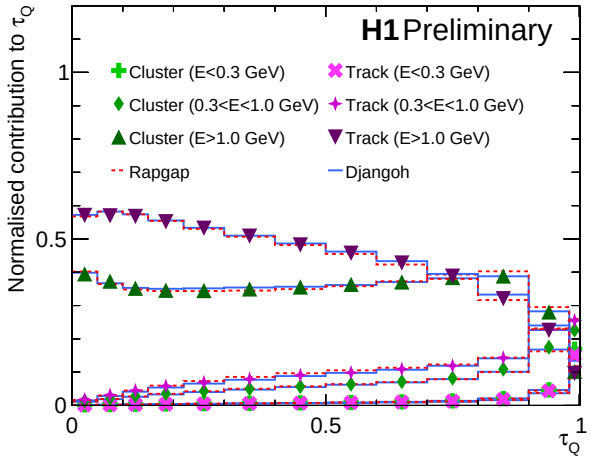

Figure 5: The normalised contribution to τ_Q for different ranges of particle energies E and for differently reconstructed particle candidates. Further details are given in the caption of fig. 4.

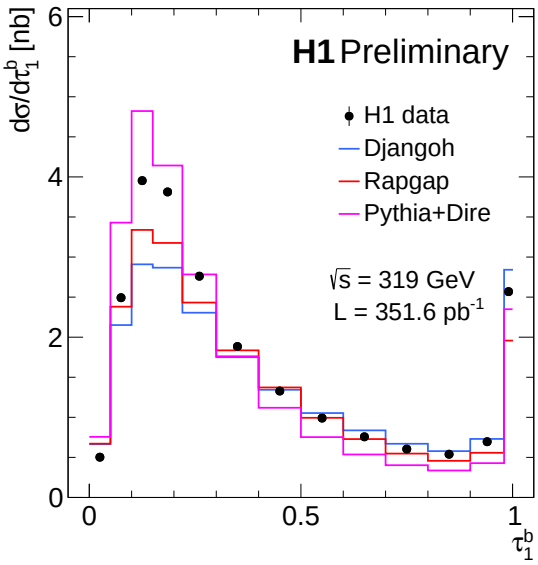

Figure 6: The differential cross section $d\sigma/d\tau_1^b$ in the kinematic region $150 < Q^2 < 20\,000\,\mathrm{GeV}^2$ and $0.2 < y < 0.7$. The data are corrected for detector effects (acceptance, resolution) and QED radiative effects. The statistcial and systematic uncertainties (vertical error bars) are commonly smaller than the marker size. The systematic uncertainties are about 5 % and dominated by the luminosity uncertainty of 2.7 % (not displayed). The data are compared to the MC predictions from Djangoh, Rapgap and Pythia, where the latter is displayed for two distinct parton-shower model Vincia and Dire (see text).

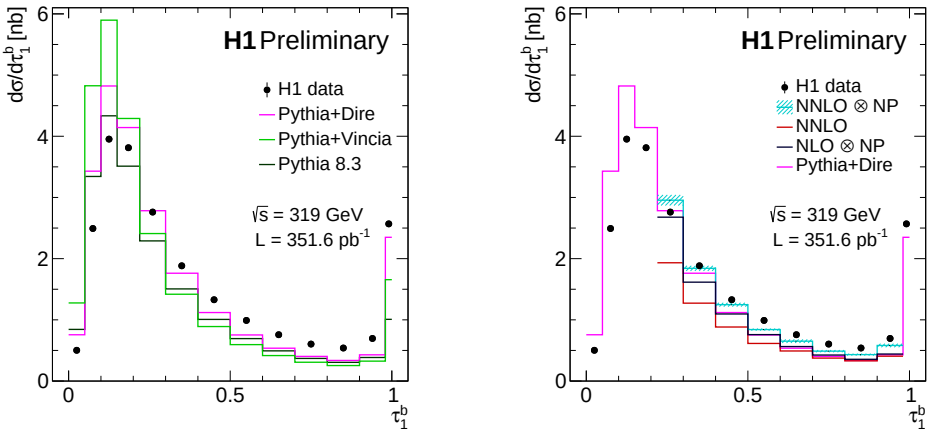

Figure 7: The differential cross section $d\sigma/d\tau_1^b$ in the kinematic region $150 < Q^2 < 20\,000\,\mathrm{GeV}^2$ and $0.2 < y < 0.7$. The data are compared to predictions from recent MC generators (left) and to fixed order calculations (right). More details on these are given in the text.

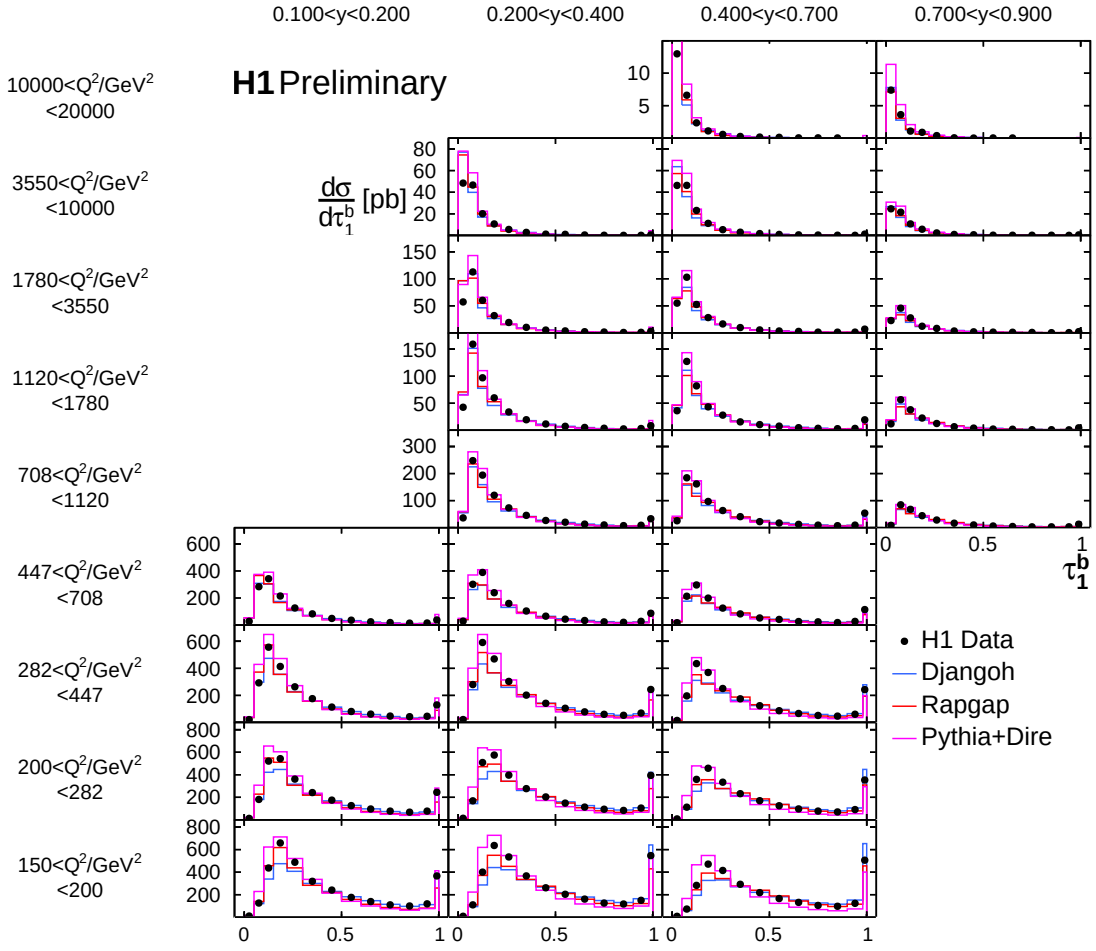

Figure 8: The differential cross section $d\sigma/\tau_1^b$ for adjacent regions in Q^2 and y (also denoted as *triple-differential* cross sections). The Q^2 and y ranges are displayed on the left and top, respectively. Every panel displays the differential cross section $d\sigma/\tau_1^b$ in that phase space. The data are compared to predictions from the Djangoh and Rapgap MC generators, where QED radiative effects were switched off. Predictions from Pythia8.3 using the Dire parton shower model are further displayed.

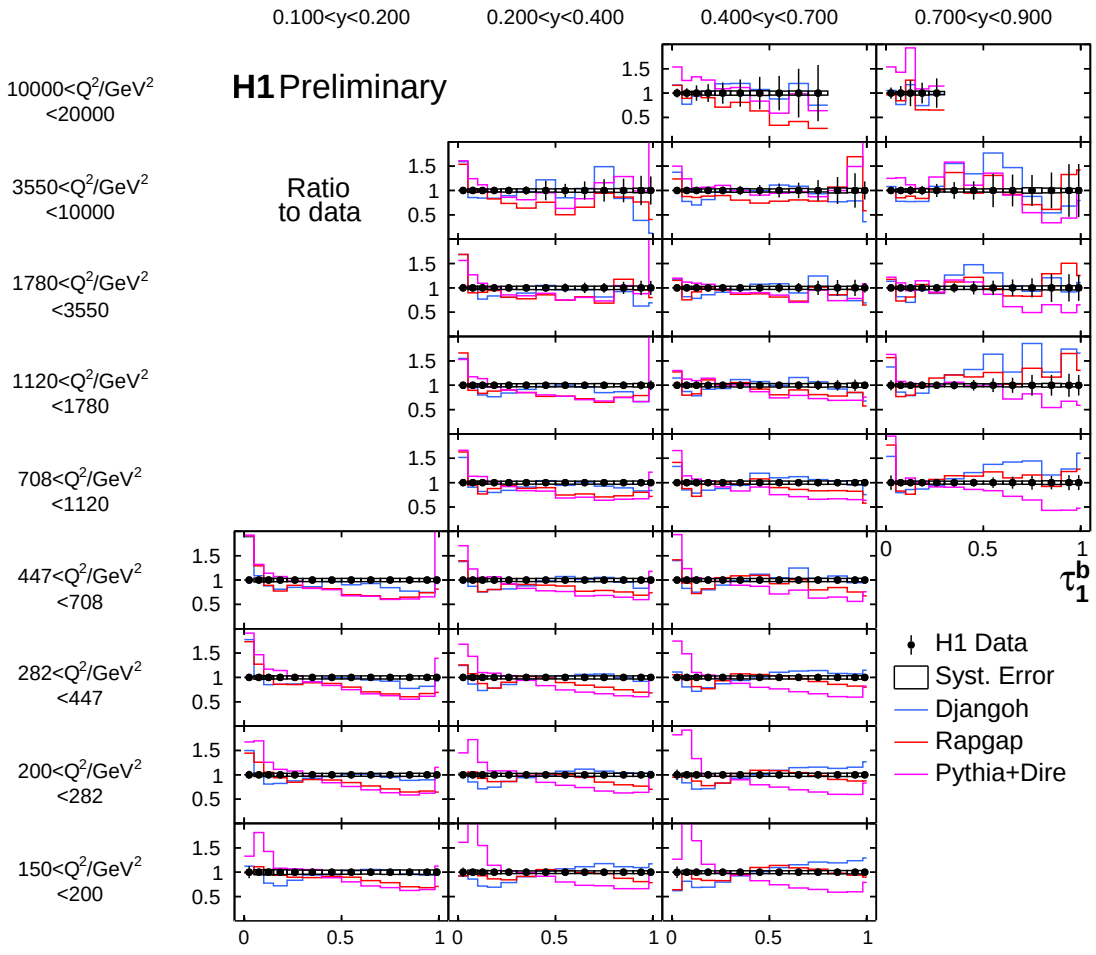

Figure 9: The ratio of the predictions to the differential cross section $d\sigma/\tau_1^b$ for adjacent regions in Q^2 and y (compare fig. 8 for more details). The black boxes indicate the size of the systematic uncertainties.

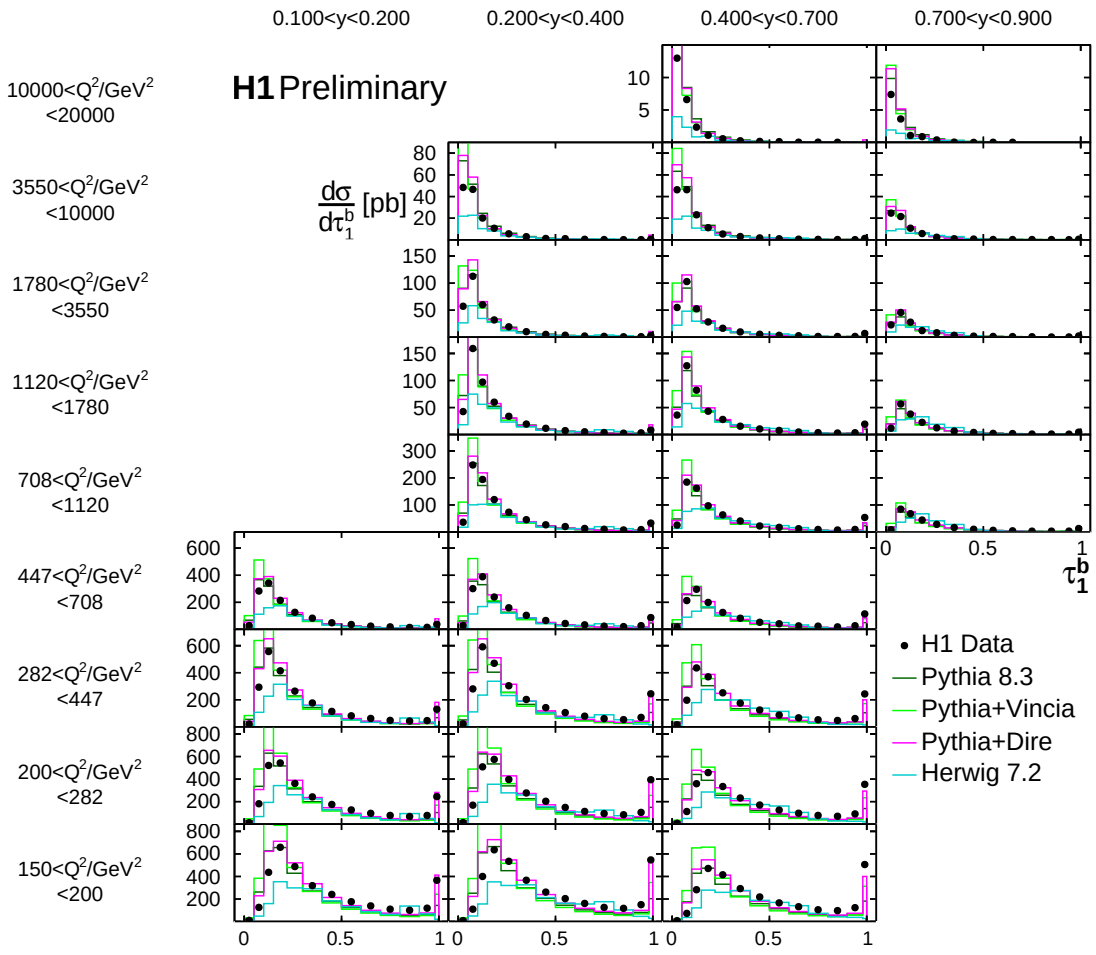

Figure 10: Similar as fig. 8, but the data are compared to predictions from recent MC generators Pythia 8.3 and Herwig 7.2. For Pythia, furthermore three different parton shower models, the 'default' shower (no label), Vincia or Dire, are displayed.

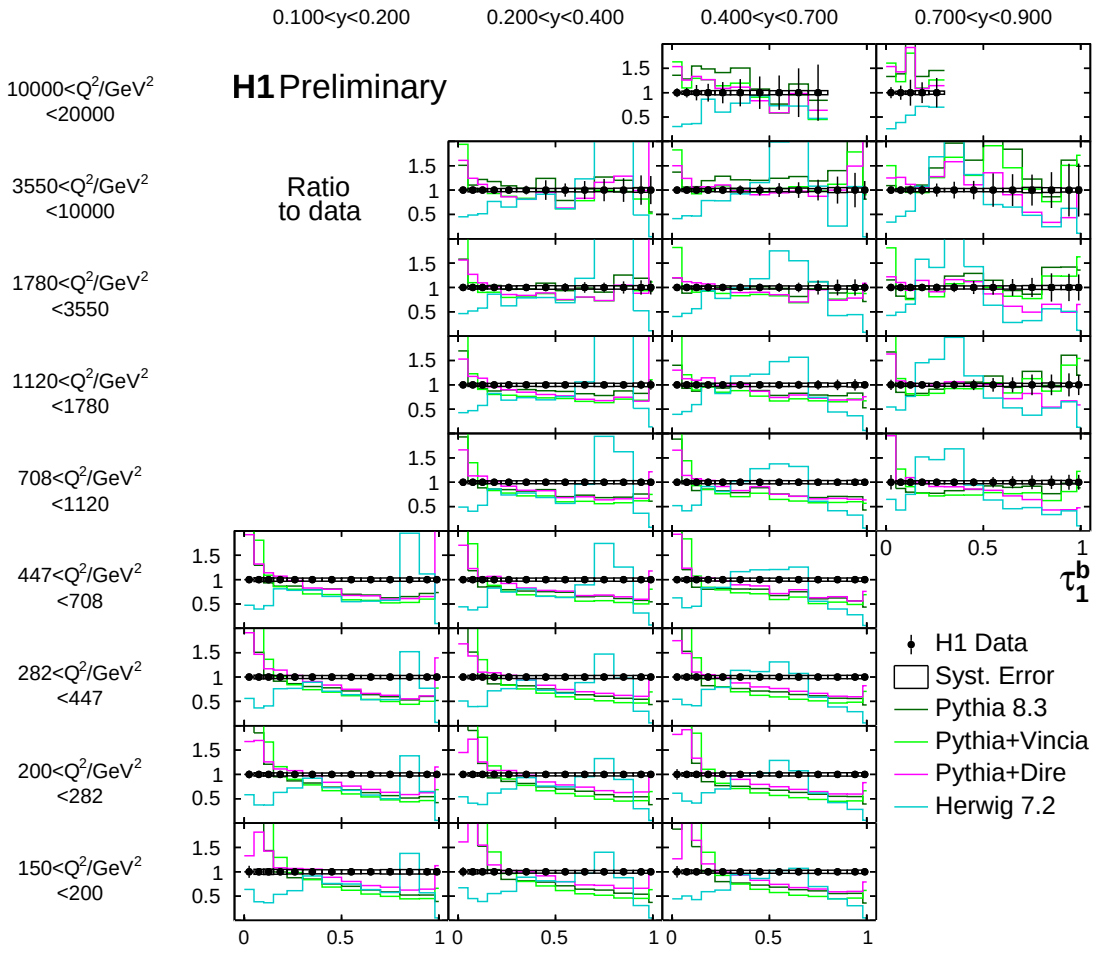

Figure 11: The ratio of the predictions (recent MC generators, as displayed in fig. 10) to the cross sections $d\sigma/d\tau_1^b$ (c.f. caption of fig. 8).

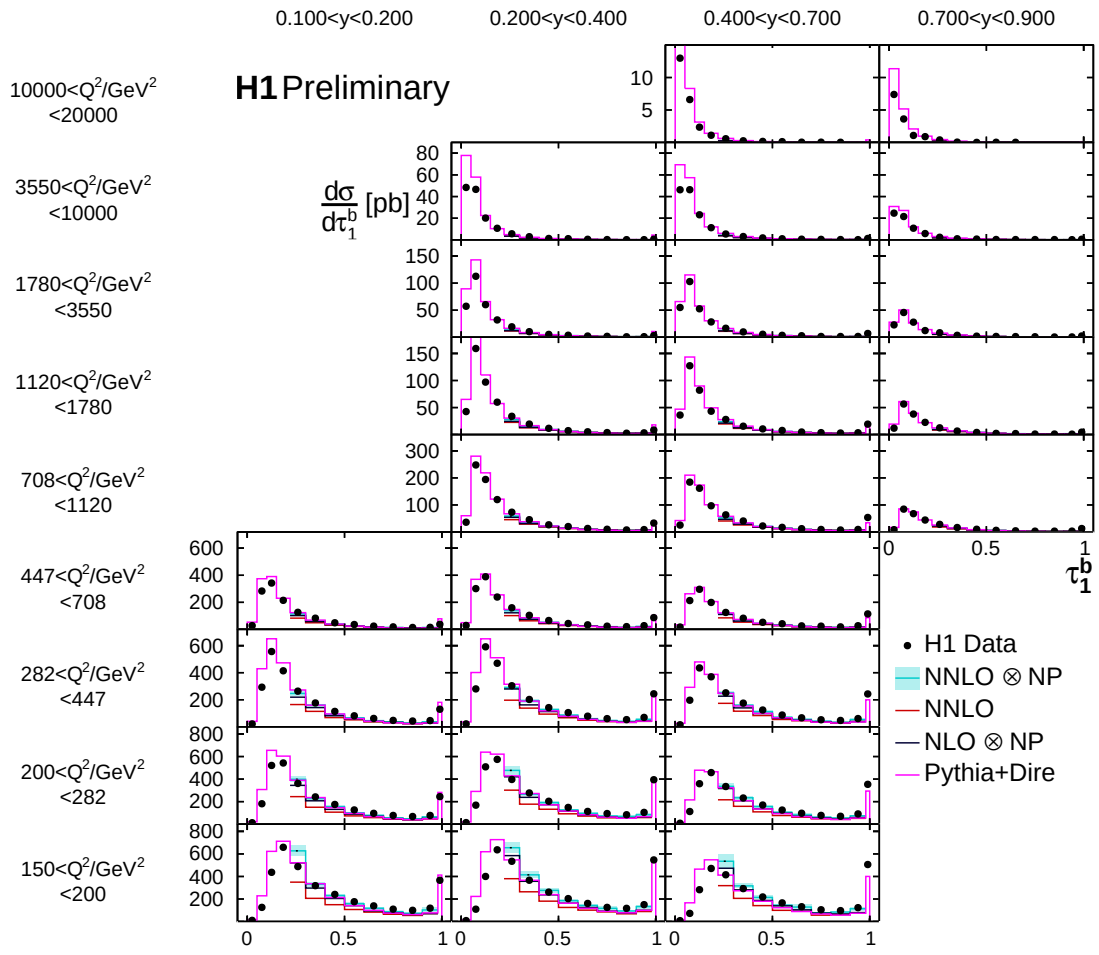

Figure 12: Similar as fig. 8, but the data are compared to predictions from a fixed order calcuation in next-to-leading order perturbative QCD (NLO) of the process $ep \to e + 2\text{jets} + X$. The NLO predictions are multiplied with hadronisation corrections (NP), which were obtained from Pythia 8.3.

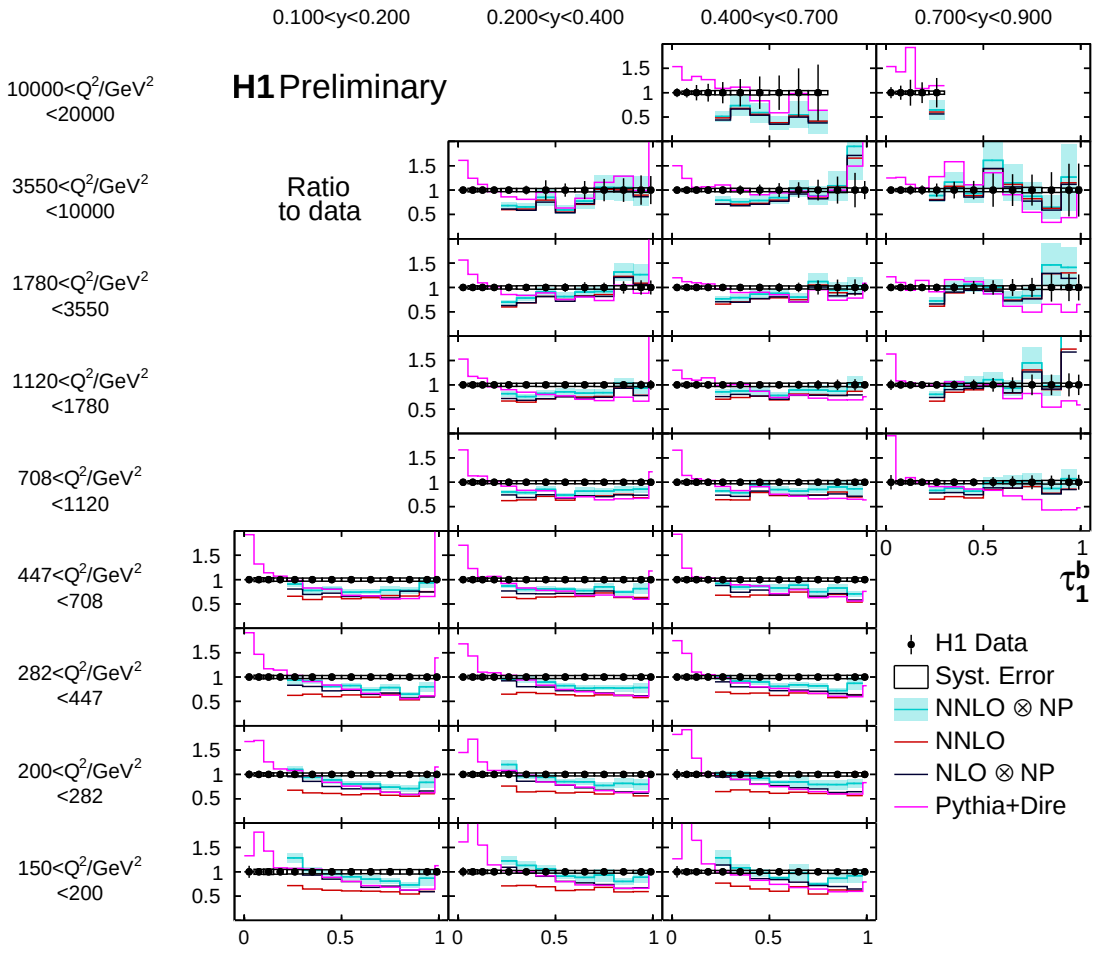

Figure 13: The ratio of the predictions (fixed order predictions, as displayed in fig. 12) to the cross sections $d\sigma/d\tau_1^b$ (c.f. caption of fig. 8).

References

[1] H1 Collaboration, C. Adloff *et al.*, "Measurement of event shape variables in deep inelastic e p scattering,", *Phys. Lett. B* 406 (1997) 256–270, arXiv:hep-ex/9706002.

[2] H1 Collaboration, C. Adloff *et al.*, "Investigation of power corrections to event shape variables measured in deep inelastic scattering,", *Eur. Phys. J. C* 14 (2000) 255–269, arXiv:hep-ex/9912052. [Erratum: Eur.Phys.J.C 18, 417–419 (2000)].

[3] H1 Collaboration, A. Aktas *et al.*, "Measurement of event shape variables in deep-inelastic scattering at HERA,", *Eur. Phys. J. C* 46 (2006) 343–356, arXiv:hep-ex/0512014.

[4] ZEUS Collaboration, S. Chekanov *et al.*, "Measurement of event shapes in deep inelastic scattering at HERA,", *Eur. Phys. J. C* 27 (2003) 531–545, arXiv:hep-ex/0211040.

[5] ZEUS Collaboration, S. Chekanov *et al.*, "Event shapes in deep inelastic scattering at HERA,", *Nucl. Phys. B* 767 (2007) 1–28, arXiv:hep-ex/0604032.

[6] P. Newman and M. Wing, "The Hadronic Final State at HERA,", *Rev. Mod. Phys.* 86 (2014) 1037, arXiv:1308.3368.

[7] K. H. Streng, T. F. Walsh and P. M. Zerwas, "Quark and Gluon Jets in the Breit Frame of Lepton - Nucleon Scattering,", *Z. Phys.* C2 (1979) 237.

[8] B. R. Webber, "Hadronic final states," in *3rd Workshop on Deep Inelastic Scattering and QCD (DIS 95)*. 4 1995. arXiv:hep-ph/9510283.

[9] V. Antonelli, M. Dasgupta and G. P. Salam, "Resummation of thrust distributions in DIS,", *JHEP* 02 (2000) 001, arXiv:hep-ph/9912488.

[10] M. Dasgupta and G. P. Salam, "Resummed event shape variables in DIS,", *JHEP* 08 (2002) 032, arXiv:hep-ph/0208073.

[11] A. Banfi, G. P. Salam and G. Zanderighi, "Principles of general final-state resummation and automated implementation,", *JHEP* 03 (2005) 073, arXiv:hep-ph/0407286.

[12] D. Kang, C. Lee and I. W. Stewart, "Using 1-Jettiness to Measure 2 Jets in DIS 3 Ways,", *Phys. Rev.* D88 (2013) 054004, arXiv:1303.6952.

[13] D. Kang, C. Lee and I. W. Stewart, "Analytic calculation of 1-jettiness in DIS at $\mathcal{O}(\alpha_s)$,", *JHEP* 11 (2014) 132, arXiv:1407.6706.

[14] H1 Collaboration, F. D. Aaron *et al.*, "Determination of the Integrated Luminosity at HERA using Elastic QED Compton Events,", *Eur. Phys. J. C* 72 (2012) 2163, arXiv:1205.2448. [Erratum: Eur.Phys.J.C 74, 2733 (2012)].

[15] H1 Collaboration, V. Andreev *et al.*, "Measurement of multijet production in ep collisions at high Q^2 and determination of the strong coupling α_s,", *Eur. Phys. J.* C75 (2015) 65, arXiv:1406.4709.

[16] H1 Collaboration, F. D. Aaron *et al.*, "Inclusive Deep Inelastic Scattering at High Q^2 with Longitudinally Polarised Lepton Beams at HERA,", *JHEP* 1209 (2012) 061, arXiv:1206.7007.

[17] R. Kogler, *Measurement of jet production in deep-inelastic e p scattering at HERA*. PhD thesis, Hamburg U., 2011.

[18] U. Bassler and G. Bernardi, "On the kinematic reconstruction of deep inelastic scattering at HERA: The Sigma method,", *Nucl. Instrum. Meth.* A361 (1995) 197–208, arXiv:hep-ex/9412004.

[19] U. Bassler and G. Bernardi, "Structure function measurements and kinematic reconstruction at HERA,", *Nucl. Instrum. Meth.* A426 (1999) 583–598, arXiv:hep-ex/9801017.

[20] K. Charchula, G. A. Schuler and H. Spiesberger, "Combined QED and QCD radiative effects in deep inelastic lepton - proton scattering: The Monte Carlo generator DJANGO6,", *Comput. Phys. Commun.* 81 (1994) 381–402.

[21] H. Jung, "Hard diffractive scattering in high-energy e p collisions and the Monte Carlo generator RAPGAP,", *Comput. Phys. Commun.* 86 (1995) 147–161.

[22] R. Brun, F. Bruyant, M. Maire, A. C. McPherson and P. Zanarini, "GEANT3,", .

[23] A. Kwiatkowski, H. Spiesberger and H. J. Mohring, "Heracles: An Event Generator for *ep* Interactions at HERA Energies Including Radiative Processes: Version 1.0,", *Comput. Phys. Commun.* 69 (1992) 155–172.

[24] T. Sjöstrand, "High-energy physics event generation with PYTHIA 5.7 and JETSET 7.4,", *Comput. Phys. Commun.* 82 (1994) 74–90.

[25] T. Sjöstrand, L. Lönnblad and S. Mrenna, "PYTHIA 6.2: Physics and manual,", arXiv:hep-ph/0108264.

[26] A. Courau and P. Kessler, "QED Compton scattering in high-energy electron - proton collisions,", *Phys. Rev.* D46 (1992) 117–124.

[27] T. Abe, "GRAPE dilepton (Version1.1): A Generator for dilepton production in e p collisions,", *Comput. Phys. Commun.* 136 (2001) 126–147, arXiv:hep-ph/0012029.

[28] H1 Collaboration, I. Abt *et al.*, "The H1 detector at HERA,", *Nucl. Instrum. Meth.* A386 (1997) 310–347.

[29] H1 Collaboration, I. Abt *et al.*, "The Tracking, calorimeter and muon detectors of the H1 experiment at HERA,", *Nucl. Instrum. Meth.* A386 (1997) 348–396.

[30] H1 SPACAL Group Collaboration, R. D. Appuhn *et al.*, "The H1 lead / scintillating fiber calorimeter,", *Nucl. Instrum. Meth.* A386 (1997) 397–408.

[31] D. Pitzl *et al.*, "The H1 silicon vertex detector,", *Nucl. Instrum. Meth. A* 454 (2000) 334–349, arXiv:hep-ex/0002044.

[32] H1 Collaboration, F. D. Aaron *et al.*, "Inclusive Deep Inelastic Scattering at High Q^2 with Longitudinally Polarised Lepton Beams at HERA,", *JHEP* 09 (2012) 061, arXiv:1206.7007.

[33] L. Lonnblad, "ARIADNE version 4: A Program for simulation of QCD cascades implementing the color dipole model,", *Comput. Phys. Commun.* 71 (1992) 15–31.

[34] B. Andersson, G. Gustafson, G. Ingelman and T. Sjöstrand, "Parton Fragmentation and String Dynamics,", *Phys. Rept.* 97 (1983) 31–145.

[35] T. Sjöstrand, "PYTHIA 5.7 and JETSET 7.4: Physics and manual,", arXiv:hep-ph/9508391.

[36] ALEPH Collaboration, R. Barate *et al.*, "Studies of quantum chromodynamics with the ALEPH detector,", *Phys. Rept.* 294 (1998) 1–165.

[37] J. Pumplin, D. R. Stump, J. Huston, H. L. Lai, P. M. Nadolsky and W. K. Tung, "New generation of parton distributions with uncertainties from global QCD analysis,", *JHEP* 07 (2002) 012, arXiv:hep-ph/0201195.

[38] T. Sjöstrand, S. Ask, J. R. Christiansen, R. Corke, N. Desai, P. Ilten, S. Mrenna, S. Prestel, C. O. Rasmussen and P. Z. Skands, "An introduction to PYTHIA 8.2,", *Comput. Phys. Commun.* 191 (2015) 159–177, arXiv:1410.3012.

[39] The Pythia authors, "Pythia 8.3 documentation," 2021. https://pythia.org.

[40] NNPDF Collaboration, R. D. Ball *et al.*, "Parton distributions from high-precision collider data,", *Eur. Phys. J. C* 77 (2017) 663, arXiv:1706.00428.

[41] W. T. Giele, D. A. Kosower and P. Z. Skands, "A simple shower and matching algorithm,", *Phys. Rev. D* 78 (2008) 014026, arXiv:0707.3652.

[42] W. T. Giele, D. A. Kosower and P. Z. Skands, "Higher-Order Corrections to Timelike Jets,", *Phys. Rev. D* 84 (2011) 054003, arXiv:1102.2126.

[43] W. T. Giele, L. Hartgring, D. A. Kosower, E. Laenen, A. J. Larkoski, J. J. Lopez-Villarejo, M. Ritzmann and P. Skands, "The Vincia Parton Shower,", *PoS* DIS2013 (2013) 165, arXiv:1307.1060.

[44] N. Fischer, S. Prestel, M. Ritzmann and P. Skands, "Vincia for Hadron Colliders,", *Eur. Phys. J.* C76 (2016) 589, arXiv:1605.06142.

[45] S. Höche and S. Prestel, "The midpoint between dipole and parton showers,", *Eur. Phys. J. C* 75 (2015) 461, arXiv:1506.05057.

[46] S. Höche and S. Prestel, "Triple collinear emissions in parton showers,", *Phys. Rev. D* 96 (2017) 074017, arXiv:1705.00742.

[47] S. Höche, F. Krauss and S. Prestel, "Implementing NLO DGLAP evolution in Parton Showers,", *JHEP* 10 (2017) 093, arXiv:1705.00982.

[48] J. Bellm *et al.*, "Herwig 7.0/Herwig++ 3.0 release note,", *Eur. Phys. J. C* 76 (2016) 196, arXiv:1512.01178.

[49] C. Bierlich *et al.*, "Robust Independent Validation of Experiment and Theory: Rivet version 3,", *SciPost Phys.* 8 (2020) 026, arXiv:1912.05451.

[50] A. Gehrmann-De Ridder, T. Gehrmann, E. W. N. Glover, A. Huss and T. A. Morgan, "The NNLO QCD corrections to Z boson production at large transverse momentum,", *JHEP* 07 (2016) 133, arXiv:1605.04295.

[51] J. Currie, T. Gehrmann, A. Huss and J. Niehues, "NNLO QCD corrections to jet production in deep inelastic scattering,", *JHEP* 07 (2017) 018, arXiv:1703.05977. [Erratum: JHEP 12, 042 (2020)].

[52] J. Currie, T. Gehrmann and J. Niehues, "Precise QCD predictions for the production of dijet final states in deep inelastic scattering,", *Phys. Rev. Lett.* 117 (2016) 042001, arXiv:1606.03991.

[53] T. Gehrmann, A. Huss, J. Mo and J. Niehues, "Second-order QCD corrections to event shape distributions in deep inelastic scattering,", *Eur. Phys. J. C* 79 (2019) 1022, arXiv:1909.02760.

[54] H1 Collaboration, V. Andreev *et al.*, "Measurement of Jet Production Cross Sections in Deep-inelastic ep Scattering at HERA,", *Eur. Phys. J. C* 77 (2017) 215, arXiv:1611.03421.

[55] S. Kluth, "Tests of Quantum Chromo Dynamics at e+ e- Colliders,", *Rept. Prog. Phys.* 69 (2006) 1771–1846, arXiv:hep-ex/0603011.